Integrated Aeroservoelastic Analysis Capability with X-29A Comparisons

K. K. Gupta,* M. J. Brenner,† and L. S. Voelker‡
NASA Ames Research Center, Edwards, California

An extension of the program STARS (a general-purpose structural analysis program) has been developed. This extension implements a complete aeroservoelastic analysis capability. Previous capabilities included finite-element modeling as well as statics, buckling, vibration, dynamic response, and flutter analyses. The authors describe the STARS program, formulate the fundamental aeroservoelasticity equations therein, and provide examples of dynamic, aeroelastic, and aeroservoelastic analyses pertaining to the X-29A aircraft. These examples include summaries of vibration and flutter analysis results obtained by the conventional *k* method and the velocity root-contour solution. Finally, selected open- and closed-loop aeroservoelastic analysis results, based on a hybrid formulation, are compared with wind-tunnel and flight test data to illustrate, using the calculated frequency responses, the dynamic interactions of structures, aerodynamics, and flight controls.

Nomenclature

$A_e(k_i)$	= aerodynamic matrix, calculated for given Mach number M_∞ and k_i values
$\hat{A}_0, \hat{A}_1, \hat{A}_2$	= equivalent aerodynamic stiffness, damping, and inertia matrices, respectively
$\hat{A}_{2+j}$	= forces due to aerodynamic lags
C_D	= damping matrix
i	= imaginary number $\sqrt{-1}$
K	= elastic stiffness matrix
k_i	= reduced frequency $\omega b/V$, ω and b being the natural frequency and wing semichord length, respectively
M	= inertia matrix
NL	= order of Padé polynomials
$P(t)$	= external forcing function
q	= displacement vector
Q	= dynamic pressure denoted as $\rho V^2/2$, ρ and V being the air density and true airspeed, respectively
s	= Laplace variable ($i\omega$)
$(V/b)\,\beta_j$	= location of the Padé pole; proper choice of lag terms β_j is important to ensure accurate fit of coefficients of the $A_e(k_i)$ matrix

Introduction

THE computer program STARS (Structures, Aerodynamics, and Related aeroservoelastic systems analysis), which is an extension of an earlier version,[1] has been designed to perform aeroservoelastic (ASE) stability analyses in addition to integrated structural modeling and vibration, flutter, and divergence analyses. Several available computer routines are expected to generally perform various facets of these analyses.[2–5] However, it was deemed advantageous to carefully reprogram and integrate current and advanced analytical formulations into a single compact, modular, interactive, and highly graphics-oriented computer program.

The authors present results from a series of correlation analyses that were performed to validate the STARS program through comparison with previously documented[4] results using other techniques. The X-29A forward-swept-wing aircraft was chosen for analysis as being representative of a modern high-performance aircraft exhibiting complex aero-structural-control interactions.

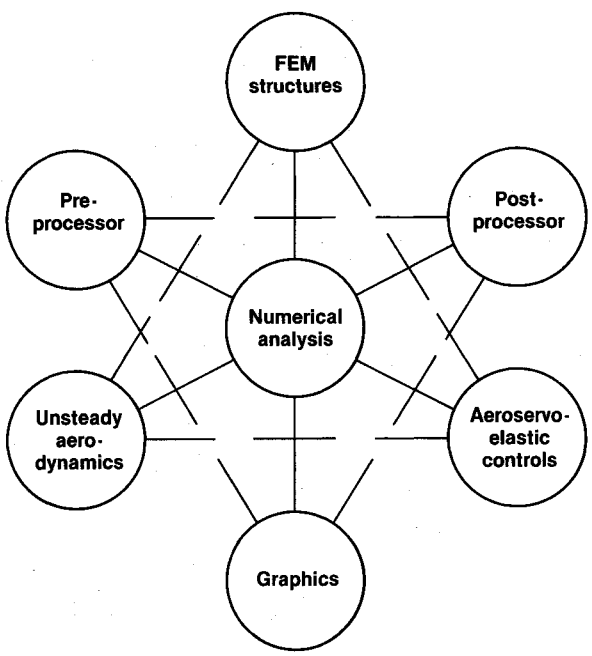

Fig. 1 Major modules and capabilities of STARS.

Presented as Paper 87-0907 at the AIAA Dynamics Specialists' Conference, Monterey, CA, April 9–10, 1987; received Aug. 3, 1987; revision received April 23, 1988. This paper is declared a work of the U.S. Government and therefore is in the public domain.

*Chief Engineer, Integrated Systems Analysis, Dryden Flight Research Facility. Member AIAA.

†Aerospace Engineer, Dryden Flight Research Facility. Member AIAA.

‡Aerospace Engineer, Dryden Flight Research Facility.

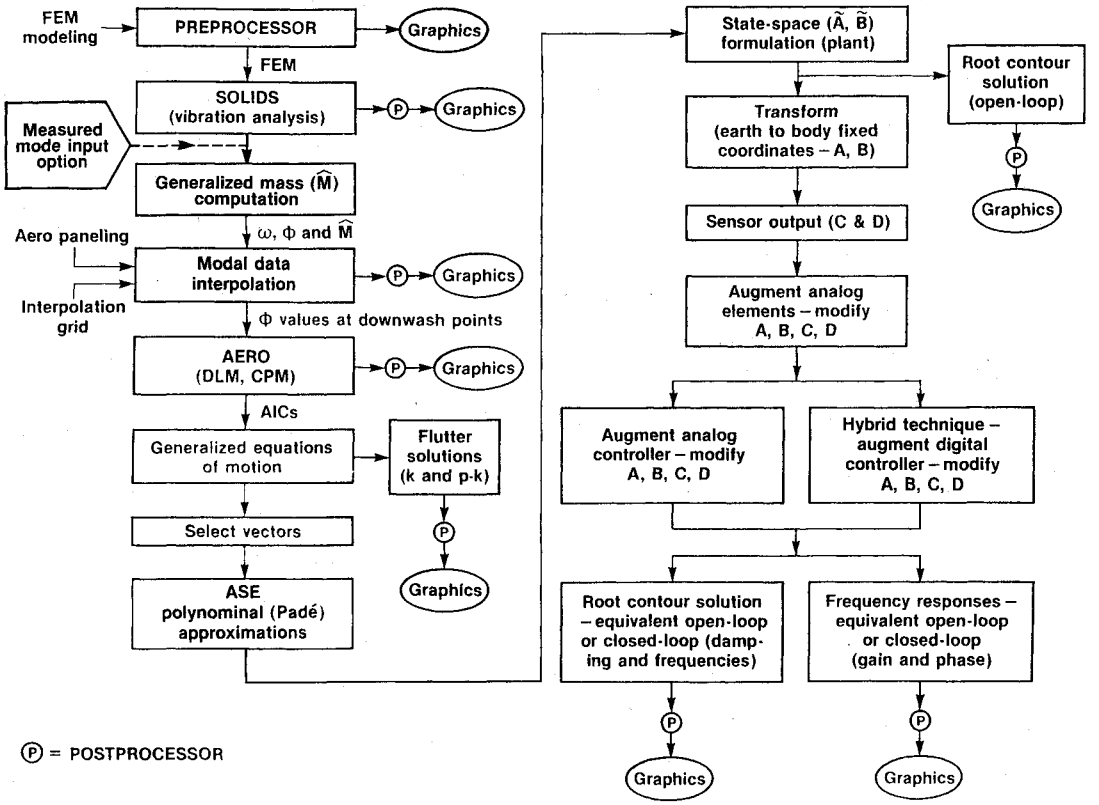

Fig. 2 STARS ASE analysis flowchart.

STARS Program Description

The various primary modules of the STARS program along with a list of major capabilities are shown in Fig. 1. A schematic of the associated dynamic aeroelastic and aeroservoelastic analyses is depicted in Fig. 2. A short description of the primary modules follows.

The preprocessor and finite-element modules permit efficient generation of very large and detailed analytical models of complicated structures from a comprehensive library of finite elements. The numerical analysis module contains advanced sparse-matrix solvers for very large order statics (Cholesky-Gaussian elimination) and dynamics problems (block Lanczos[1,7] algorithms for undamped structures and combined Sturm sequence/inverse iteration[8] for structures with viscous and structural damping). These solution procedures permit the structure to have combined prestressed, spinning, and nonspinning components and can perform the full spectrum of statics, buckling, vibration, and forced dynamic response analyses of analytical models containing up to several thousand degrees of freedom with relatively modest computer resources.

The unsteady aerodynamics module is capable of computing unsteady aerodynamic forces for both subsonic and supersonic flows in the frequency domain and performing the flutter solutions. Currently the doublet lattice method (DLM), the constant pressure method (CPM), and the Mach box (MB) technique are operational. Both the k and p-k (see Ref. 6) flutter solution methods are available.

The aeroservoelasticity module recasts the aerostructural problem into the Laplace domain, including curve fitting the unsteady aerodynamics using Padé and least-squares approximations, generating the appropriate state-space matrices including the flight control system, and performing the inertial to body-fixed coordinate transformations. This module also performs open-loop stability analyses (velocity root contour) and both open- and closed-loop frequency response analyses for continuous and hybrid systems.

The postprocessor module provides an extensive capability for plotting all analysis results on a wide variety of graphics terminals.

Numerical Formulation

The equations of motion of a structure such as an aircraft may be written as

$$\boldsymbol{K}\boldsymbol{q} + \boldsymbol{C}_D\dot{\boldsymbol{q}} + \boldsymbol{M}\ddot{\boldsymbol{q}} + Q\boldsymbol{A}_e(k_i)\boldsymbol{q} = \boldsymbol{P}(t) \tag{1}$$

which is general in nature. The STARS program uses a recently developed block Lanczos eigenproblem solution routine[7] to solve the associated free-vibration problem

$$\boldsymbol{K}\boldsymbol{q} + \boldsymbol{M}\ddot{\boldsymbol{q}} = \boldsymbol{0} \tag{2}$$

to yield the desired roots ω and vectors $\boldsymbol{\Phi}$. A coordinate transformation of the form

$$\boldsymbol{q} = \boldsymbol{\Phi}\boldsymbol{\eta} \tag{3}$$

when applied to Eq. (1) yields

$$\boldsymbol{\Phi}^T\boldsymbol{M}\boldsymbol{\Phi}\ddot{\boldsymbol{\eta}} + \boldsymbol{\Phi}^T\boldsymbol{C}_D\boldsymbol{\Phi}\dot{\boldsymbol{\eta}} + \boldsymbol{\Phi}^T\boldsymbol{K}\boldsymbol{\Phi}\boldsymbol{\eta} + Q\boldsymbol{\Phi}^T\boldsymbol{A}_e(k_i)\boldsymbol{\Phi}\boldsymbol{\eta} = \boldsymbol{\Phi}^T\boldsymbol{P}(t) \tag{4}$$

which may be written as

$$\hat{\boldsymbol{M}}\ddot{\boldsymbol{\eta}} + \hat{\boldsymbol{C}}_D\dot{\boldsymbol{\eta}} + \hat{\boldsymbol{K}}\boldsymbol{\eta} + Q\hat{\boldsymbol{A}}_e(k_i)\boldsymbol{\eta} = \hat{\boldsymbol{P}}(t) \tag{5}$$

where the generalized coordinate $\boldsymbol{\eta} = \lfloor \boldsymbol{\eta}_R\ \boldsymbol{\eta}_\varepsilon\ \boldsymbol{\eta}_\delta \rfloor$ and the modal matrix $\boldsymbol{\Phi} = [\boldsymbol{\Phi}_R\ \boldsymbol{\Phi}_\varepsilon\ \boldsymbol{\Phi}_\delta]$, incorporating rigid-body, elastic, and control surface motions, respectively.

Each coefficient of the generalized aerodynamic force matrix in the Laplace domain may next be expressed as Padé polynomials[9] in ik (or sb/V) as follows:

$$\hat{\boldsymbol{A}}_e(k_i) = \hat{\boldsymbol{A}}_0 + \left(\frac{sb}{V}\right)\hat{\boldsymbol{A}}_1 + \left(\frac{sb}{V}\right)^2\hat{\boldsymbol{A}}_2 + \sum_{j=1}^{NL}\frac{\hat{\boldsymbol{A}}_{2+j}s}{s + \frac{V}{b}\beta_j} \cdots \tag{6}$$

The coefficients $\hat{A}_0, \hat{A}_1, \hat{A}_2, \ldots$ are determined by least-squares solution using the aerodynamic coefficient data $[\hat{A}_e(k_i)]$ for a number of k_i values.

Substituting Eq. (6) into Eq. (5), with $\hat{P}(t) = \mathbf{0}$, collecting like terms and assuming two lag terms results in

$$(\hat{K} + Q\hat{A}_0)\eta + \left(\hat{C}_D + Q\frac{b}{V}\hat{A}_1\right)s\eta + \left(\hat{M} + \frac{b^2}{V^2}\hat{A}_2\right)s^2\eta + Q\hat{A}_3\left(\frac{s}{s + \frac{V}{b}\beta_1}\right)\eta + Q\hat{A}_4\left(\frac{s}{s + \frac{V}{b}\beta_2}\right)\eta = \mathbf{0} \tag{7}$$

which may be written as

$$\tilde{K}\eta + \tilde{C}_D s\eta + \tilde{M}s^2\eta + Q\hat{A}_3 x_1 + Q\hat{A}_4 x_2 = \mathbf{0} \tag{8a}$$

and furthermore, the following relationship may also be established

$$\dot{x}_1 = -\frac{V}{b}\beta_1 x_1 + \dot{\eta} \tag{8b}$$

$$\dot{x}_2 = -\frac{V}{b}\beta_2 x_2 + \dot{\eta} \tag{8c}$$

These equations may be rearranged as

$$\begin{bmatrix} I & & & \\ & 0 & & \\ & \tilde{M} & & \\ & & I & \\ 0 & & & \\ & & & I \end{bmatrix} \begin{bmatrix} \dot{\eta} \\ \ddot{\eta} \\ \dot{x}_1 \\ \dot{x}_2 \end{bmatrix} = \begin{bmatrix} 0 & I & 0 & 0 \\ -\tilde{K} & -\tilde{C}_D & -Q\hat{A}_3 & -Q\hat{A}_4 \\ 0 & I & -\frac{V}{b}\beta_1 & 0 \\ 0 & I & 0 & -\frac{V}{b}\beta_2 \end{bmatrix} \begin{bmatrix} \eta \\ \dot{\eta} \\ x_1 \\ x_2 \end{bmatrix} \tag{9}$$

where I is the identity matrix. Equation (9) may be written as

$$M'\dot{X}' = K'X' \tag{10}$$

which may further be arranged as

$$\dot{X}' = (M')^{-1}K'X' \tag{11a}$$

$$\equiv RX' \tag{11b}$$

in which the state-space vector can also be written as

$$X' = \lfloor(\eta_R\ \eta_e\ \dot{\eta}_R\ \dot{\eta}_e\ x_1\ x_2)(\eta_\delta\ \dot{\eta}_\delta)\rfloor \tag{12a}$$

$$= \lfloor \tilde{x}\ u \rfloor \tag{12b}$$

where the control mode states are separated as the vector u.

Equation (11b) can then be written as

$$\begin{bmatrix} \dot{\tilde{X}} \\ \dot{u} \end{bmatrix} = \begin{bmatrix} R_{I,I} & R_{I,II} \\ R_{II,I} & R_{II,II} \end{bmatrix} \begin{bmatrix} \tilde{X} \\ u \end{bmatrix} \tag{13}$$

in which the first set of equations denotes the dynamics of the plant while the second set represents the dynamics of the control modes. Considering only the plant dynamics, the state-space equations become

$$\dot{\tilde{X}} = \tilde{A}\tilde{X} + \tilde{B}u \tag{14}$$

in which $\tilde{A}$ is the plant dynamics matrix and similarly $\tilde{B}$ is the control surface influence matrix. A coordinate transformation is required to transform the state matrices from an earth-fixed to a body-fixed coordinate system to enable the incorporation of control laws and feedback. Since no transformations are applied to elastic and aerodynamic lag stage vectors, a transformation of the form

$$\dot{X} = \tilde{T}_2^{-1}(\hat{A}\tilde{T}_1 - \tilde{T}_3)X + \tilde{T}_2^{-1}\hat{B}u$$

$$= AX + Bu \tag{15}$$

in which

$$\tilde{T}_1 = \begin{bmatrix} T_1 & 0 \\ 0 & I \end{bmatrix}$$

T_1 being a relevant coordinate transformation matrix yields the required state-space equation in the body coordinate system; extensive details of the procedure are given in Gupta et al.[10]

A sensor interpolation matrix T_s deriving displacement, velocity, and acceleration from structural data is developed next; when applied to Eq. (15), it results in the equation for output y containing the sensor motion q_s and its derivatives as follows:

$$y = CX + Du \tag{16}$$

with

$$y = \begin{bmatrix} q_s \\ \dot{q}_s \\ \ddot{q}_s \end{bmatrix}, \quad C = \begin{bmatrix} C_0 \\ C_2 \end{bmatrix}, \quad D = \begin{bmatrix} 0 \\ D_2 \end{bmatrix}$$

$$C_0 = [T_s\Phi\ 0\ 0\ 0], \qquad C_1 = \begin{bmatrix} T_s\Phi & 0 & 0 & 0 \\ 0 & T_s\Phi & 0 & 0 \end{bmatrix}$$

$$C_2 = C_1 A. \qquad D_2 = C_1 B$$

in which C and D are matrices signifying output at the sensors due to body and control surface motions, respectively.

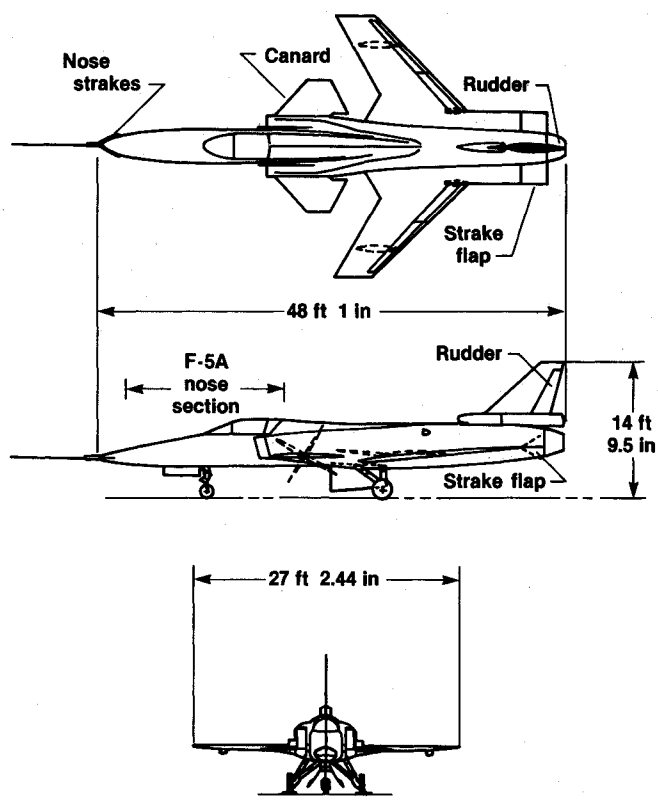

Fig. 3 X-29A aircraft.

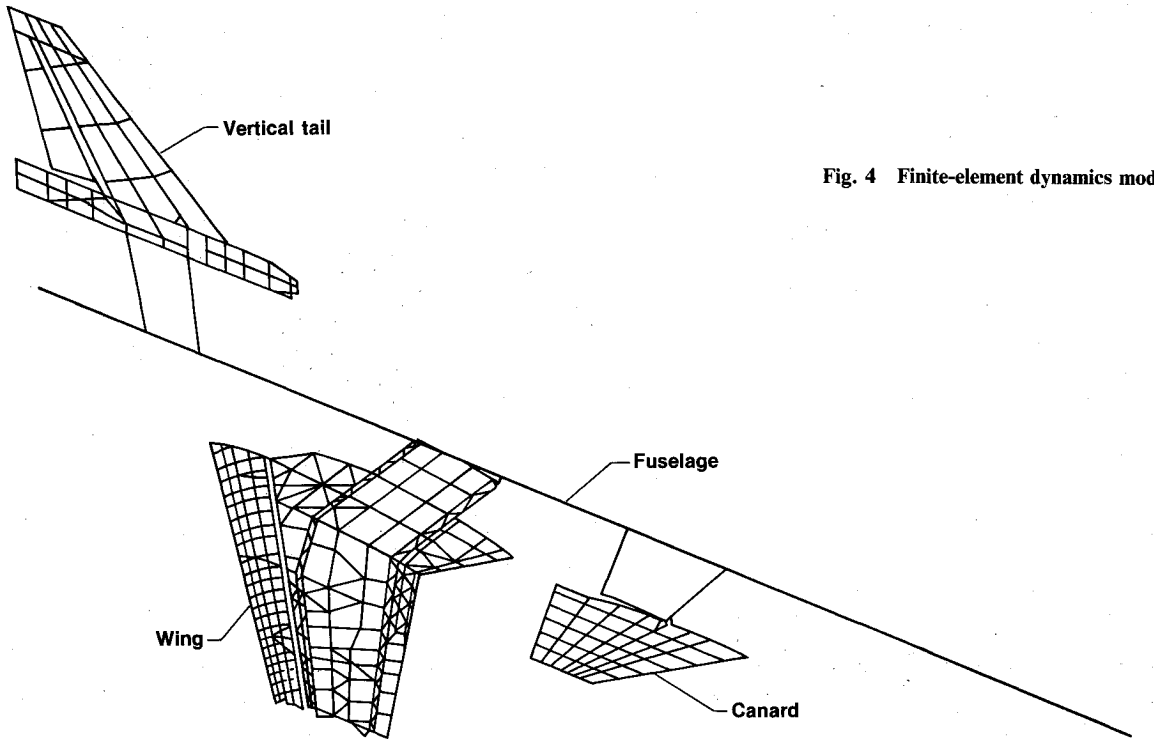

Fig. 4 Finite-element dynamics model of X-29A aircraft.

The aeroelastic stability analysis involves solution of the eigenvalue problem

$$|A - \lambda I| = 0 \tag{17}$$

for various dynamic pressures. An instability of the system (flutter) is indicated by a change in sign, from negative to positive, of the real part of an eigenvalue λ. If the corresponding frequency, being the imaginary part of the root, also approaches the zero value, it is indicative of divergence.

To obtain frequency response characteristics of an aircraft with a feedback control system, a Laplace transformation is first applied to the state-space equations, from which the open-loop transfer function $G(s)$ is easily derived as

$$y(s) = G(s)u(s) \tag{18}$$

where

$$G(s) = C[sI - A]^{-1}B + D \tag{19}$$

is the desired expression and $s = \alpha + i\omega$, α being the damping term. In the presence of controller $H(s)$, the closed-loop transfer function $\hat{G}(s)$ is derived from the relation

$$y(s) = \hat{G}(s)r(s) \tag{20}$$

where

$$\hat{G}(s) = G(s)[I + H(s)G(s)]^{-1} \tag{21}$$

and $r(s)$ is the reference input.

The matrix inversion involved in Eq. (19) for each value of s is laborious and can be avoided by first solving the eigenvalue problem for matrix A and then effecting a coordinate transformation. This results in the following expression for the open-loop transfer function:

$$G(s) = C\psi(sI - \lambda)^{-1}\psi^{-1}B + D \tag{22}$$

where λ and ψ are, respectively, the eigenvalue and eigenvector matrices of A. It may be noted that $(sI - \lambda)$ is a diagonal matrix and its inversion is trivial. Thus, calculating $G(s)$ from Eq. (22) is preferable to using Eq. (19). After the appropriate transfer functions have been formulated, the phase and gain results may be calculated and plotted as functions of frequency using standard procedures.

Numerical Results for X-29A Aircraft

The unique features of the X-29A forward-swept-wing research aircraft[11,12] (Fig. 3) include a very thin and flexible forward-swept wing, aeroelastically tailored with advanced composite wing covers designed to elastically eliminate structural divergence without a weight penalty. The supercritical airfoil provides efficient transonic cruise performance and high transonic maneuvering capability. Full-authority variable-incidence canards operate with full-span variable-camber (double-hinged) flaperons and strake flaps to achieve minimum trim drag. With the canards, the vehicle is up to 35% statically unstable, requiring appropriate feedback flight controls for augmented static stability. These technologies, when combined, can result in significant improvement in aerodynamic performance and structural efficiency, but without proper integration can also result in adverse dynamic interaction of the flight controls with the flexible structure. Thus, ASE analysis is playing an increasingly important role in this integration process. Presented next are example results of elastic, aeroelastic and ASE analyses of the X-29 aircraft, as performed by STARS.

Vibration, Flutter, and Divergence Analysis

The symmetric half-model of the aircraft structure as used in STARS analysis is shown in Fig. 4. This reduced-order model (3078 degrees of freedom) was derived by the equivalent shell method from the contractor's full-stress finite-element model (approximately 7000 degrees of freedom) and was used for all of the following STARS analyses. A comparison of associated natural frequencies for the symmetric case, measured by ground vibration survey (GVS) and calculated by STARS, is given in Table 1. The typical symmetric flutter and divergence solution results obtained by the contractor using GVS modal data and the STARS analytical results are compared in Table

Table 1 X-29A aircraft vibration frequency comparison (symmetric case)

Mode	GVS-measured frequency, Hz	STARS (calculated) Frequency, Hz	STARS (calculated) Difference, %
Wing first bending (W1B)	8.61	8.96	+4.1
Fuselage first bending (F1B)	11.65	12.87	+10.5
Fuselage second bending (F2B)	24.30	19.03	−21.7
Canard pitch (CP)	21.07	21.02	−0.2
Wing second bending (W2B)	26.30	26.28	−0.1
Wing first torsion (W1T)	36.70	30.30	−17.4
Canard bending pitch (CBP)	42.20	47.70	+13.0
Wing third bending (W3B)	51.50	49.52	−3.8

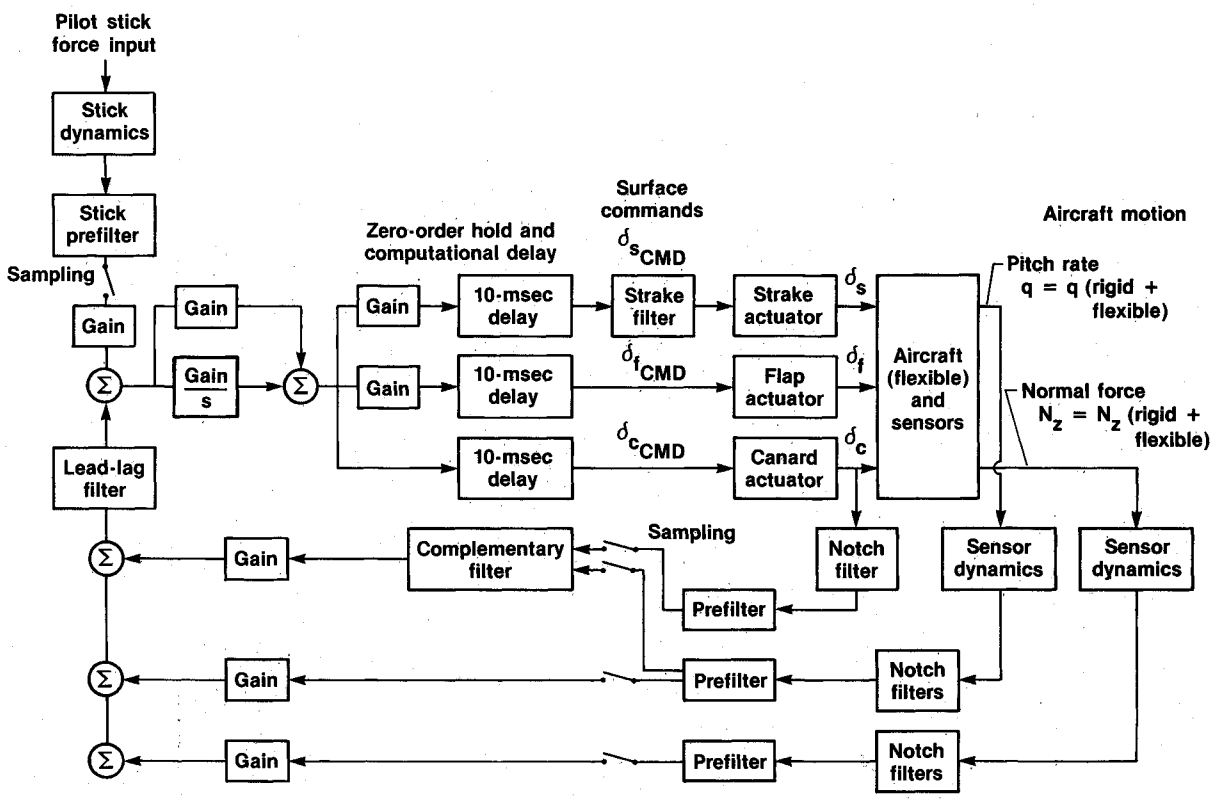

Fig. 5 X-29A normal mode longitudinal axis control law basic stability loop.

2; similar analyses were also performed for the antisymmetric case.

Aeroservoelastic Controls Analysis

To study the interaction between aeroelastic dynamics and a control system, the plant matrices are augmented with the control system elements. The plant consists of rigid-body states, elastic structural modes, and two unsteady aerodynamic lag states. The sensed measurements include rigid-body and flexible effects. The sensed states are fed back to the control system, as in Fig. 5, in the X-29A basic longitudinal axis control law.[4]

In the X-29A analysis, analog and digital control laws are augmented with the plant to compute both time histories and frequency responses. The closed-loop coupled airframe-flight control system can be represented by state equations to generate time histories, which in the digital case are known only at discrete time intervals corresponding to the sample rate. To account for aliasing effects upon discretization in the frequency domain, a hybrid frequency response technique[13] is used to model digital elements in the s plane.

Table 2 Comparison of calculated flutter speeds for the X-29A aircraft (symmetric case)

Instability	Crossing mode	Critical speed, KEAS: STARS modes, k method	Critical speed, KEAS: STARS modes, Root-contour method	Critical speed, KEAS: Contractor GVS, k method
Divergence	(W1B)	838.10	833.50	808.00
Divergence	(CP)	913.01	917.91	980.00
Flutter	(F1B)	848.06	797.31	924.00
Flutter	(W2B)	1142.95	1156.98	1315.00

The hybrid frequency response technique was applied to compute the frequency responses of the X-29A normal digital mode[4] augmented with a wind tunnel-based steady aerodynamic model, and STARS unsteady, flexible dynamics. The equivalent open-loop frequency responses of the digital mode

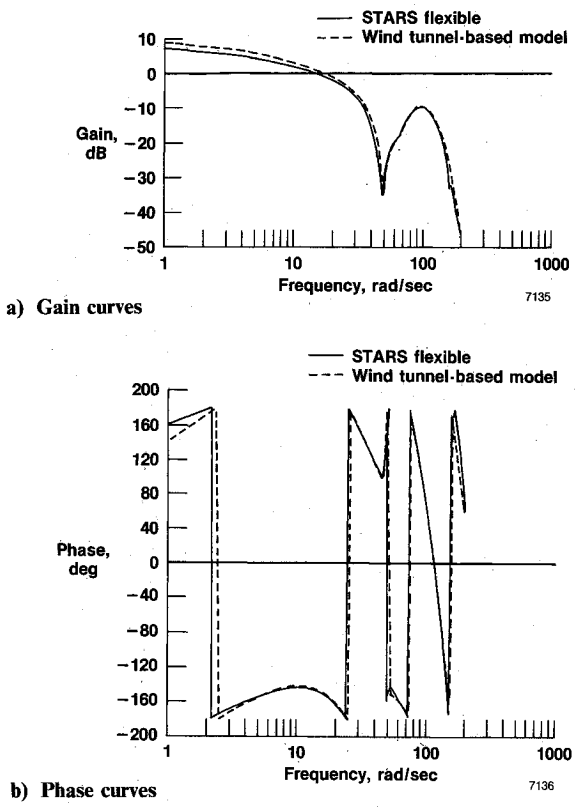

Fig. 6 Equivalent open-loop frequency responses for X-29A normal digital mode; STARS flexible and wind-tunnel dynamics (Mach 0.9; density ratio 1.0).

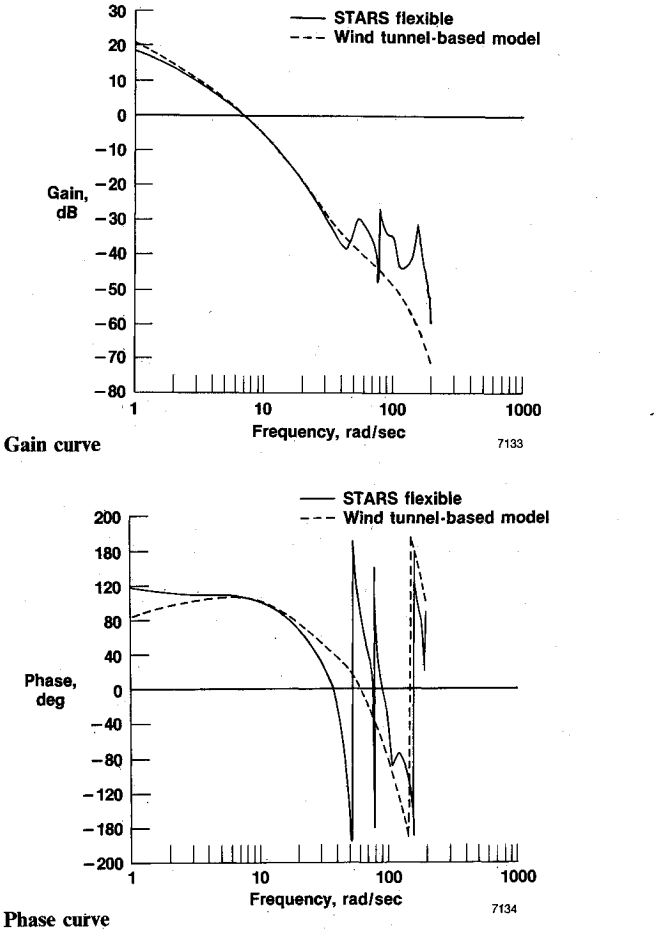

Fig. 7 Closed-loop frequency responses for X-29A normal digital mode; STARS flexible and wind-tunnel dynamics (Mach 0.9, density ratio 1.0).

and the STARS analytical unsteady, flexible dynamics referenced to the controller augmented with wind tunnel-based steady aerodynamics are shown in Fig. 6. The associated closed-loop responses from stick position to sensed normal force are shown in Fig. 7. In the closed-loop response, the first two structural modes are observable below the Nyquist frequency of 126 rad/s, and no aliasing problem due to higher frequency modes is apparent since the gain curves match exceedingly well below the first structural mode frequency of approximately 54 rad/s. In this case, aliasing would exhibit very lightly damped false dynamics that were checked and found to be nonexistent. A typical comparison of X-29A flight-measured closed-loop modal damping and frequency values with those computed by the STARS program is shown in Fig. 8. These comparisons for the fully augmented aircraft dynamics indicate the accurate prediction capability of the STARS program.

When the loops are closed, analysis of stability and control with aerostructural effects is possible. For instance, preliminary analyses may show that an ASE instability involving the flexible modes may exist for a particular feedback flight control system design. Further analyses, with notch filters included, would confirm or deny filter effectiveness in suppressing the instability without unduly degrading the rigid-body gain and phase margins. Physical relocation of feedback sensors may also be studied as an alternative approach to minimizing the flexible effects of feedback measurements on the rigid-body control laws. When both flexible and rigid-body stability are satisfactorily achieved, the control system structure may then be further modified to meet performance and sensitivity conditions for body-axis control.

Future Research Activities

The STARS aero module has recently been upgraded to include the constant pressure method.[14] This procedure was selected for its improvement over the Mach box technique and for its applicability to unsymmetric structures such as the

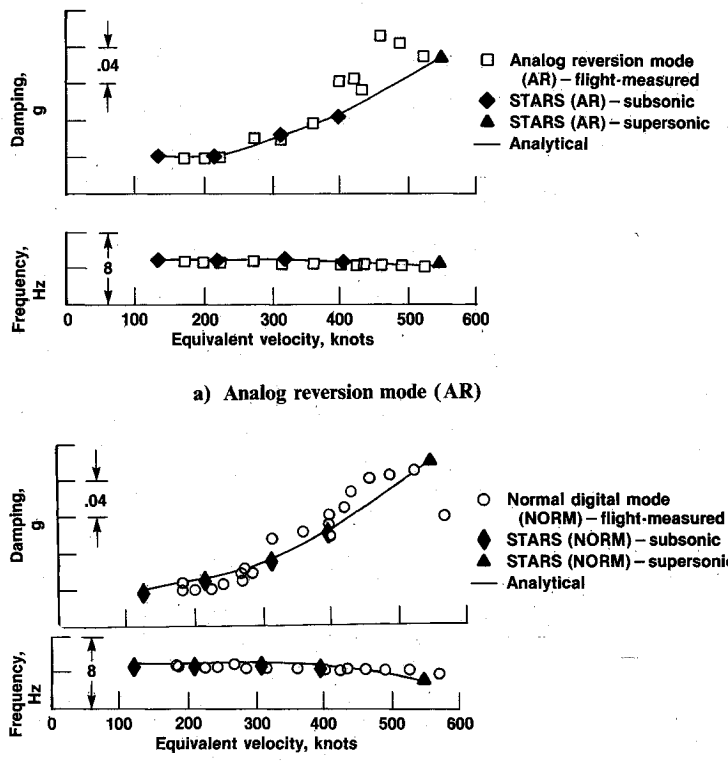

Fig. 8 Comparison of X-29A closed-loop modal damping and frequencies between flight-measured data and STARS for symmetric first bending mode at 20,000 ft.

oblique-wing research aircraft.[15] Also, because of current advances in the solution of structural eigenvalue problems,[7,8] it is intended to use a detailed finite-element stress model of the X-29A aircraft for future modal analyses. This is expected to produce more accurate results compared with usual analyses performed by using reduced-order dynamics models.

References

[1]Gupta, K. K., "STARS—A General-Purpose Finite-Element Computer Program for Analysis of Engineering Structures," NASA RP-1129, 1984.

[2]"The NASTRAN Theoretical Manual," NASA SP-221(06), 1981.

[3]Noll, T., Blair, M., and Cerra, J., "ADAM—An Aeroservoelastic Analysis Method for Analog or Digital Systems," *Journal of Aircraft*, Vol. 23, Nov. 1986, pp. 852–858.

[4]Zislin, A., Laurie, E., Wilkinson, K., and Goldstein, R., "X-29 Aeroservoelastic Analysis and Ground Test Validation Procedures," AIAA Paper 85-3091, Oct. 1985.

[5]Taylor, R. F., Miller, K. L., and Brockman, R. A., "A Procedure for Flutter Analysis of FASTOP-3 Compatible Mathematical Models, Vol. I—Theory and Application," Air Force Wright Aeronautical Labs., TR81-3063, June 1981.

[6]Hassig, H. J., "An Approximate True Damping Solution of the Flutter Equation by Determinant Iteration," *Journal of Aircraft*, Vol. 8, Nov. 1971, pp. 885–889.

[7]Gupta, K. K. and Lawson, C. L., "Implementation of a Block Lanczos Algorithm for Eigenproblem Solution of Gyroscopic Systems," AIAA Paper 87-0946, April 1987.

[8]Gupta, K. K., "Formulation of Numerical Procedures for Dynamic Analysis of Spinning Structures," *International Journal of Numerical Methods Engineering*, Vol. 23, Dec. 1986, pp. 2347–2357.

[9]Abel, I., "An Analytical Technique for Predicting the Characteristics of a Flexible Wing Equipped With an Active Flutter-Suppression System and Comparison With Wind-Tunnel Data," NASA TP-1367, 1979.

[10]Gupta, K. K., Brenner, M. J., and Voelker, L. S., "Development and Application of an Integrated Aeroservoelastic Analysis Program," NASA TP, in press, 1988.

[11]Sefic, W. J. and Maxwell, C. M., "X-29A Technology Demonstrator Flight Test Program Overview," NASA TM-86809, 1986.

[12]Whitaker, A. and Chin, J., "X-29 Digital Flight Control System Design," AGARD-CP-384, Active Control Systems—Review, Evaluation, and Projections, Oct. 1984.

[13]Whitback, R. F., Didaleusky, D. G. J., and Hofmann, L. G., "Frequency Response of Digitally Controlled Systems," *Journal of Guidance Control*, Vol. 4, July–Aug. 1981, pp. 423–427.

[14]Appa, K., "Constant Pressure Panel Method for Supersonic Unsteady Airload Analysis," *Journal of Aircraft*, Vol. 24, Oct. 1987, pp. 696–702.

[15]Gregory, T., "Oblique Wing Ready for Research Aircraft," *Aerospace America*, Vol. 23, June 1985, pp. 78–81.